EXPERIMENTAL AND ANALYTICAL COMPARISON OF STIFF AND FLEXIBLE ROTOR BLADES FOR TILTROTOR WHIRL-FLUTTER STABILITY

Andrew R. Kreshock, U. S. Army Combat Capabilities Development Command, Army Research Laboratory, Hampton, VA, USA
Robert P. Thornburgh, U. S. Army Combat Capabilities Development Command, Army Research Laboratory, Hampton, VA, USA
Hao Kang, U. S. Army Combat Capabilities Development Command, Army Research Laboratory, Aberdeen Proving Ground, MD, USA
Hyeonsoo Yeo, U. S. Army Combat Capabilities Development Command, Aviation & Missile Center, Moffett Field, CA, USA

ABSTRACT

The U.S. Army and NASA recently completed their second wind tunnel entry in the Transonic Dynamics Tunnel with the TiltRotor Aeroelastic Stability Testbed (TRAST). Parametric studies were conducted on important components of the wing semi-span testbed and 8-ft-diameter rotor system to assess their effect on whirl flutter. TRAST is a dynamically scaled testbed that is representative of the XV-15 and has adjustable pitch-flap coupling (δ_3), tuning springs, and two blade sets with different stiffnesses. The first blade set, made of fiberglass, is dynamically scaled to the XV-15 blade so that the frequencies are approximate to the aircraft. The second blade set replaces the fiberglass layup with carbon fiber and has approximately twice the stiffness. This paper will show how a dynamically tuned blade can increase the stability boundary.

1. INTRODUCTION

Whirl-flutter stability has been a subject of interest for decades, first stemming from a pair of Lockheed Electra propeller aircraft that crashed (Ref. 1), followed by early tiltrotor designs (Ref. 2). These developments led to the XV-15 (Ref. 3) and finally to development of the V-22 aircraft (Ref. 4). Reed describes key differences between propeller aircraft, which lack hinges and have stiff blades, and tiltrotor aircraft, which have both flexible blades and a flap (or gimbal) response (Ref. 5).

More recent activities in tiltrotor whirl flutter are being conducted at the University of Maryland, which has completed a series of tests for both a gimballed and hingeless rotor system (Ref. 6 & 7). Additionally, NLR is leading the ATTILA Project with collaborations from other European organizations to investigate whirl flutter for the Next Generation Civil TiltRotor program (Ref. 8).

The U.S. Army, in collaboration with NASA, recently completed its second whirl-flutter test of the Tiltrotor Aeroelastic Stability Testbed (TRAST) from October to December 2023 in the NASA Langley Transonic Dynamic Tunnel. TRAST is a semi-span aeroelastic tiltrotor testbed developed by the U.S. Army and NASA to investigate whirl-flutter stability of tiltrotor aircraft (Ref. 9). Though based on the XV-15, TRAST is a generic tiltrotor testbed representative of a typical tiltrotor aircraft configuration. It is a semi-span testbed consisting of a right-hand wing, a rigid fuselage/fairing, and a pylon with an 8-ft-diameter rotor. The rotor can be driven by an electric motor or operated in windmilling mode (Figure 1). Designed for parametric studies of key control-system values and structural stiffnesses, TRAST includes a hydraulic control system for pilot control, wing excitation, and active control studies.

As a follow-on test to the first entry, detailed in Ref. 10, the second wind-tunnel test included a large parametric study of different pylon mounting stiffnesses (pitch and yaw springs), various pitch-flap angles, and different blade sets. This paper will focus on the effect of the blade structural dynamics on whirl flutter by examining the stability between two blade sets made with fiberglass and carbon fiber, which have significantly different stiffnesses. Each of these blade sets was tested with two different pitch-flap coupling angles, -15° and -30°. The test and analysis results presented here are a subset consisting of four configurations of the twelve that were tested. Analytical models (CAMRAD II and RCAS) will be used be predict the stability of the rotor system and compared against the stability measurements obtained during the wind-tunnel test for the two blade sets. Both models were extensively compared between experiment and

Presented at the 50th European Rotorcraft Forum, Marseille, France September 10–12, 2024.

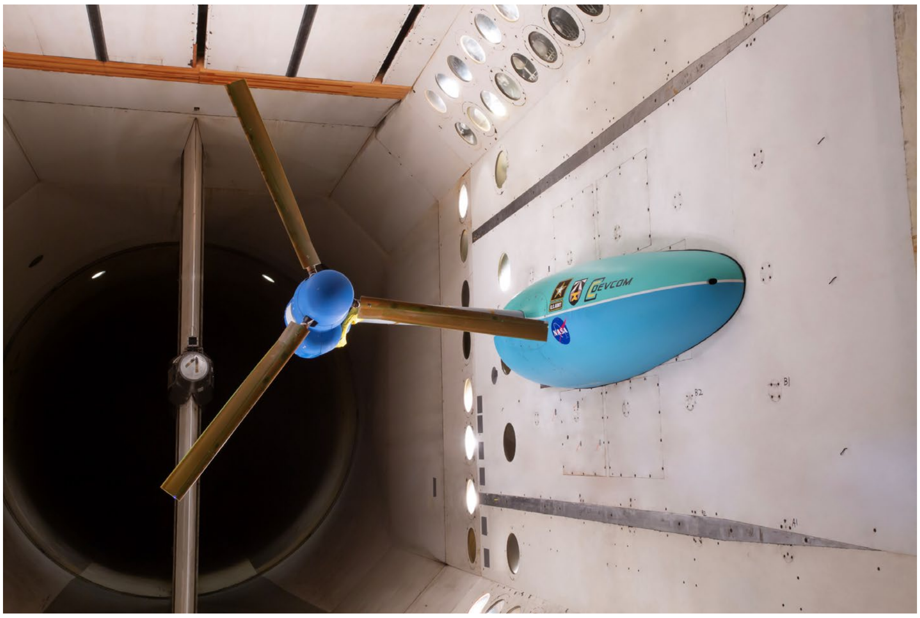

Figure 1. TRAST installed in the Langley Transonic Dynamics Tunnel with the fiberglass blade set.

NASTRAN whenever possible. Additional information on the modeling activities can be found in References 11 and 12.

1.1. Whirl Flutter Definitions / Discussions

Whirl-flutter has become a broad term to include any aeroelastic coupling of a propeller or rotor with the airframe elasticity. An attempt will be made here to define the terms more specifically. In general, there is propeller whirl flutter and gimballed tiltrotor whirl flutter, which is only applicable to vehicles like the XV-15 and V-22. However, there are different types of phenomena that get labeled as whirl flutter and therefore clear definitions will help the reader understand the nuances.

Propeller Whirl Flutter (Pitch & Yaw)

The instability in propeller aircraft historically has resulted from flexibility in the airframe and requires both pitch and yaw modes. This instability occurs despite the relative rigidity of the blades and hub. This type of instability is straightforward to predict and prevent, but it is exacerbated when the two modes are close in frequency.

Tiltrotor Whirl Flutter (Flapping Rotor & Airframe Pitch)

Gimballed tiltrotors like the XV-15 have a slightly different mechanism for instability. Only one of the modes needs to be contributed from the airframe, and this mode then combines with the rotor gimbal mode so that the gimbal acts like an additional pitch or yaw mode. This is also true for articulated rotors such as those studied in the Grumman Helicat wind-tunnel test (Ref. 2). Counterintuitively, for a gimballed rotor a negative pitch-flap coupling (δ_3) is required to reduce excessive flapping. However, the use of negative δ_3 influences the frequency of the gimbal mode and couples it with the wing vertical bending mode, leading to a lower instability velocity for a higher (more negative) δ_3. Classically, positive pitch-flap coupling is defined as flap up/pitch up, but rotor aeromechanics refer to this as negative δ_3. In this document all references to pitch-flap coupling use this δ_3 definition, meaning flap up/pitch up.

Proprotor Whirl Flutter (Flapping/Blade/Airframe Pitch)

There is a second phenomenon that occurs in tiltrotor aircraft that combines the instability discussed above with the rotor lag mode flexibility. The frequency of the regressive lag mode decreases with airspeed, and at high speeds it will cross the wing vertical mode frequency. This asymmetric lag mode increases the wing damping initially, but after the lag mode frequency crosses the wing mode frequency, there is a very steep drop in the damping.

Hingeless Tiltrotor Instability

In general, a rigid hingeless tiltrotor would be akin to a propeller aircraft, but with a larger rotor and more rotating inertia. However, the large rotors of hingeless tiltrotors have significantly more flexibility than propellers to alleviate the loads induced during helicopter-mode flight, and this can often cause stability problems. Reference 13 discusses a several design cases for a few generic rotor systems mounted on the same pylon wing, Figure 2.

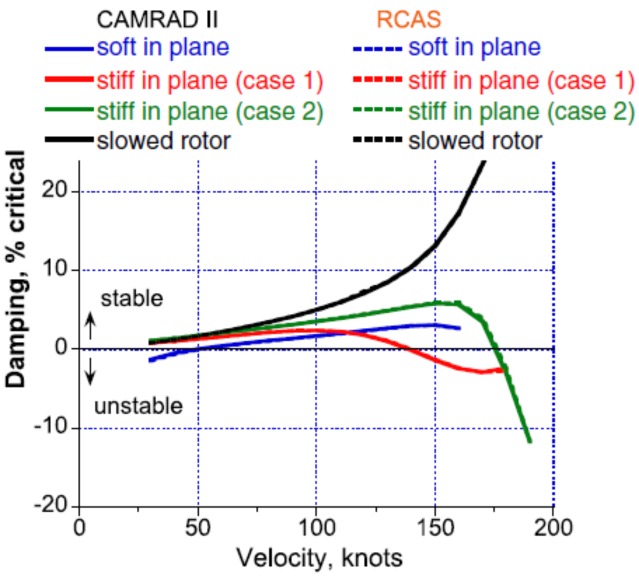

Figure 2. Hingeless tiltrotor flutter.

1.2. Analytical Modeling

The analytical TRAST model has evolved over the course of the program from a single load path model in Ref. 11 to a more detailed rotor model in Ref. 12. The current analysis starts where Ref. 12 concludes, using a dual load path rotor model and interface springs representing the pitch bearings between the blade and spindle. The wing structural model was also updated between the initial and subsequent test configurations. Structurally, the wing remains unchanged, but small modifications were made to the pylon non-structural mass to reflect physical changes to the testbed. Additionally, an assessment after the first wind tunnel test, determined that the gimbal springs were inducing additional friction in the gimbal joint. Consequently, those springs were replaced with springs 10x softer. This did not produce any significant changes in the analytical predictions since the analyses do not account for spring preload or friction. However, from testing the wing vertical bending mode damping was reduced from 2.5% to 1.2%.

2. TEST OVERVIEW

The experimental stability results presented in this paper were obtained during a wind-tunnel test of the TRAST in late 2023 at the Langley Transonic Dynamics Tunnel. This test focused on parametric studies to experimentally quantify the effect of system changes on the stability response during forward flight. As part of this testing, six different control-system pitch-flap coupling angles (δ_3) were tested at two different rotor speeds, providing an extensive characterization of pitch-flap coupling on the whirl-flutter response. In addition to the baseline rotor-blade set, which was a set of fiberglass blades areoelastically scaled to be comparable to the XV-15 blades, a second set of rotor blades was tested. This second set had an identical planform to the baseline blade set but was manufactured using carbon-fiber construction. This resulted in a blade set that was significantly stiffer than the baseline blades and provided an opportunity to experimentally demonstrate how the blade modes interact with the system modes in tiltrotor forward flight.

2.1. Blade Comparison

The TRAST testbed features two separate rotor blade sets made from the same mold and similar layup. Table 1 presents some important blade properties, including measured mass, center of gravity, and analytically derived cantilevered blade frequencies. These frequencies were further verified through experimental vibration testing on a floor mount. Table 1 also includes rotating blade frequencies. This is a single blade analysis akin to a cantilevered rotor blade, but with the hub properties included, rotating at 100% nominal rotor speed (NR, 909 RPM). Despite the similarities in weight and center of gravity (see Table 1), the frequencies from the carbon-fiber blade set are over 1.3 times higher than the fiberglass-blade set, highlighting the dynamic characteristics between the two blade sets.

Table 1. Blade comparison between the carbon-fiber and fiberglass blade sets.

		CARBON-FIBER BLADE	FREQ (/REV)	FIBERGLASS BLADE	FREQ (/REV)
	MASS, LBM	1.502		1.619	
	RADIAL CG, INCHES	22.645		22.468	
CANTILEVERED BLADE	FLAP	26.22	-	15.63	-
	LAG	49.07	-	33.28	-
SINGLE BLADE, 100% NR, 0° COLL	FLAP	30.38	2.01	23.38	1.54
	LAG	39.89	2.63	30.39	2.00

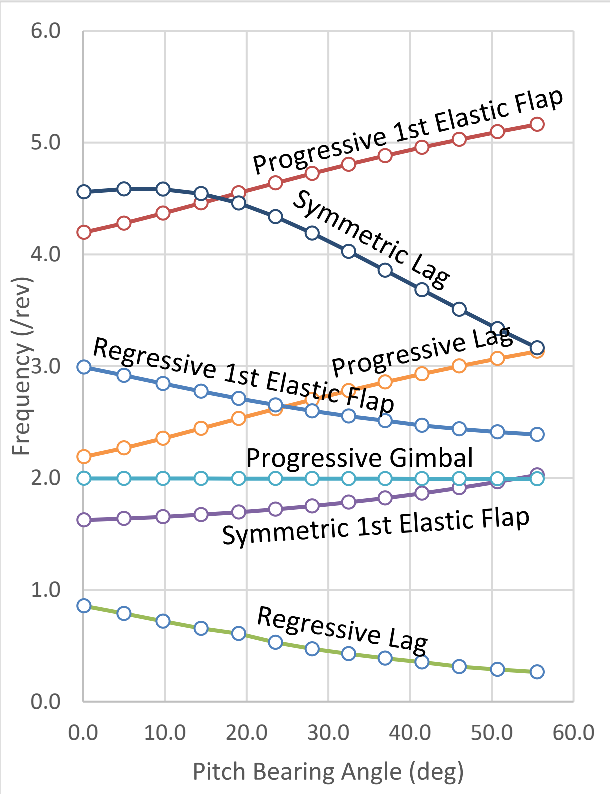

Figure 3. Fiberglass rotor frequencies at 909 RPM over a range of collective angles in a vacuum.

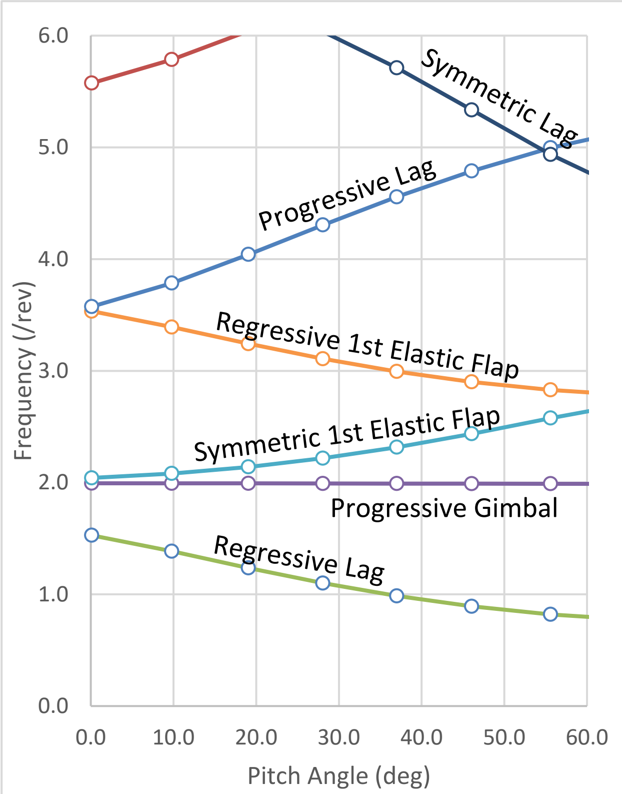

Figure 4. Carbon-fiber rotor frequencies at 909 RPM over a range of collective angles in a vacuum.

One of the most difficult issues tiltrotor aircraft designers encounters has been the number of rotor modes that exist, complicated by the fact that tiltrotors require a large collective range of motion for forward flight. Figure 3 is a plot of the rotor frequencies versus collective at the nominal helicopter rotor speed. An attempt has been made to label each mode for the fiberglass-blade set, calculated by CAMRAD II. The reader should note that these blades are highly twisted, and the term "flap" mode, which typically refers to an out-of-plane motion of the rotor, is roughly perpendicular to the chord line. Therefore, it is more accurate to describe this mode as a twisted flap mode. At high collectives, this mode shape has a range of motion aligned with the rotor plane. Another interesting feature of gimballed rotor designs is that flap modes ultimately have different boundary conditions depending on the symmetry or asymmetry of the blades. In Figure 3 the symmetric flap mode (around 1.6/rev) behaves similarly to a single blade with a cantilevered boundary condition. But the progressive/regressive flap modes ($\beta\pm1$), which are not symmetric, act similarly to blades with a pinned boundary condition and therefore have a higher frequency. The symmetric lag mode is typically around 1.5/rev; however, this mode is highly dependent on the drive shaft boundary condition. In Figure 3 the model has a free shaft boundary condition (equivalent to a pinned rotor, or wind milling), which causes this symmetric lag mode to increase to 4.5 /rev. The progressive (ζ+1) and regressive (ζ-1) lag modes, because they are not symmetrical about the shaft, act as a cantilevered boundary condition. This regressive lag mode ultimately crosses the wing vertical mode (around 5 Hz or 0.3 /rev).

Figure 4 presents the carbon-fiber rotor frequencies which are 0.5-0.8/rev higher than the corresponding fiberglass rotor frequencies. This means the regressive lag mode no longer intersects with the wing vertical mode. This difference is quite influential on the flutter boundary, as will be discussed below.

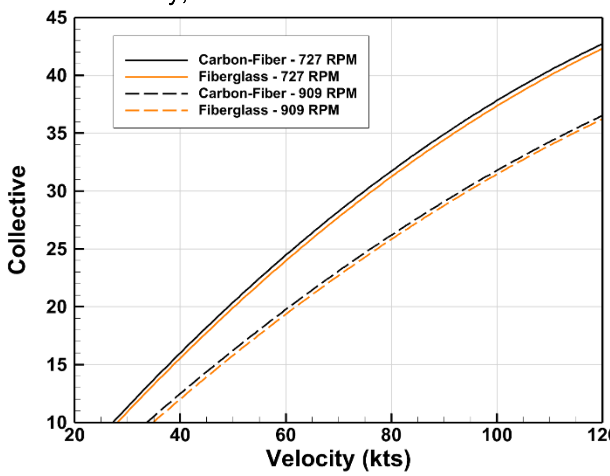

Figure 5. Collective vs Tunnel Speed (kts) for both carbon-fiber and fiberglass rotors with curve fit from test data.

Table 2. Test Matrix

		Fiberglass Rotor		Carbon-Fiber Rotor	
		727RPM	909RPM	727RPM	909RPM
Pitch-flap coupling, δ_3	-30°	4k	4k	4k	4k
	-25°	4k	4k		
	-20°	3k, 4k, 5k, 5k*	3k, 4k, 5k, 5k*		
	-15°	4k	4k	4k	4k
	-10°	4k	4k		
	-0°	4k	4k	4k	4k

Note: Pylon pitch spring is denoted in the cells. * indicates the half-stiff diaphragm spring.

One validation of the aerodynamic similarity between the two blade sets is how well they performed during the wind tunnel test. Figure 5 presents the curve fit test data of the collective pitch of the blades versus tunnel speed for the two blade sets. Ideally, since both blades were trimmed to a specific rotor speed using collective pitch for a given tunnel speed for a wind milling condition (zero torque), the carbon-fiber rotor and the fiberglass rotor would produce the same trim. The small differences seen in Figure 5 are likely due to the exact twist distribution of these highly twisted blades. This distribution difference can be the result of the manufacturing process or differences in how the two composite layups couple with the centrifugal loading of the blades.

2.2. Stability Measurements

The technique used to obtain stability measurements during this wind-tunnel test is similar to the technique detailed in Ref. 2. Once the testbed is at a steady flight condition and rotor speed, the testbed is excited by oscillating the swashplate at the frequency of the mode being measured. The aerodynamic forces induced by this oscillation create a forced response of this mode that steadily increases until it reaches a target amplitude, at which time the oscillation is ended and the free-decay response of the testbed is measured. A minimum of five free-decay measurements are performed for each mode of interest at each test condition.

The process of using the free-decay measurements to estimate the system damping is complicated by the wind-tunnel turbulence that induces quasi-random forced response on the measured system response. Traditional methods for damping estimation from free-decay signals, such as moving-block and Prony techniques, do not account for the presence of a random forced response, and this results in large scatter in their damping estimates. At higher tunnel speeds, the steady-state vibration levels created by the turbulence begin to approach the target amplitudes of the swashplate oscillations. This not only adds a large random response to the free decay, but it also results in fewer cycles before the signal level decays to below the steady-state noise floor. Thus, even averaging the five to ten points per test condition can be insufficient for accurately identifying the system damping at high tunnel speeds.

The measured damping estimates presented in the present paper are an attempt to average out the effect of turbulence more effectively. The Prony algorithm is quite effective at extracting frequency and damping from very short segments of a free decay. Over a short enough time segment, the turbulence can be considered as a random impulse on the system. Thus, by using one-cycle segments of time history and incrementing the segment along the time history with 95-percent overlap, several hundred Prony estimates can be obtained from each free-decay measurement. Averaging these one-cycle Prony estimates from all of the decay measurements at a given test condition has resulted in a more consistent estimate for the system damping than simply averaging the small number of moving-block results.

3. TEST AND ANALYSIS COMPARISON

The wind-tunnel test measured the stability of twelve independent configurations at both 100% NR and 80%. This paper focuses on four of those configurations as outlined in Table 2. Although the test conditions varied slightly throughout, the average density was around 0.002090 slug/ft^3, equivalent to approximately 1950 psf of tunnel pressure.

Figure 6 plots the frequency and damping of the wing-vertical mode (blue) and wing-in-plane mode (red) for a pitch-flap coupling of -30° at 909 RPM with the fiberglass rotor. This Figure 6 compares frequency and damping from analysis using CAMRAD II (dashed line), the test data from recent wind tunnel entry (squares) and the curve fit of that data (solid line). In this configuration the wing vertical bending mode becomes unstable around 90 knots. The analysis predicts this instability to occur around 75 knots. This represents a typical trend for the current TRAST analytical models in which the analysis often underestimates the stability boundary, but generally captures the trends. Notable shortcomings in the analysis include interpolated airfoil tables based on only four

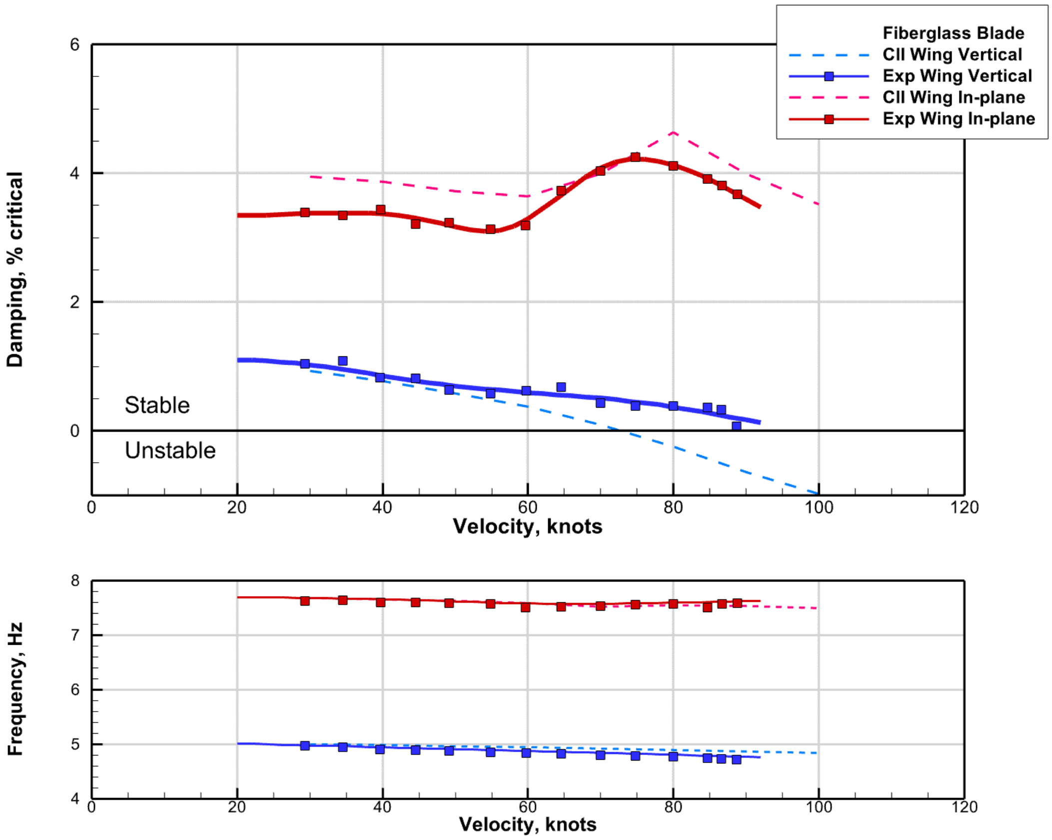

Figure 6. Frequency and damping test data and analytical results for the fiberglass rotor at 909 RPM with pitch-flap coupling (δ_3) of -30°.

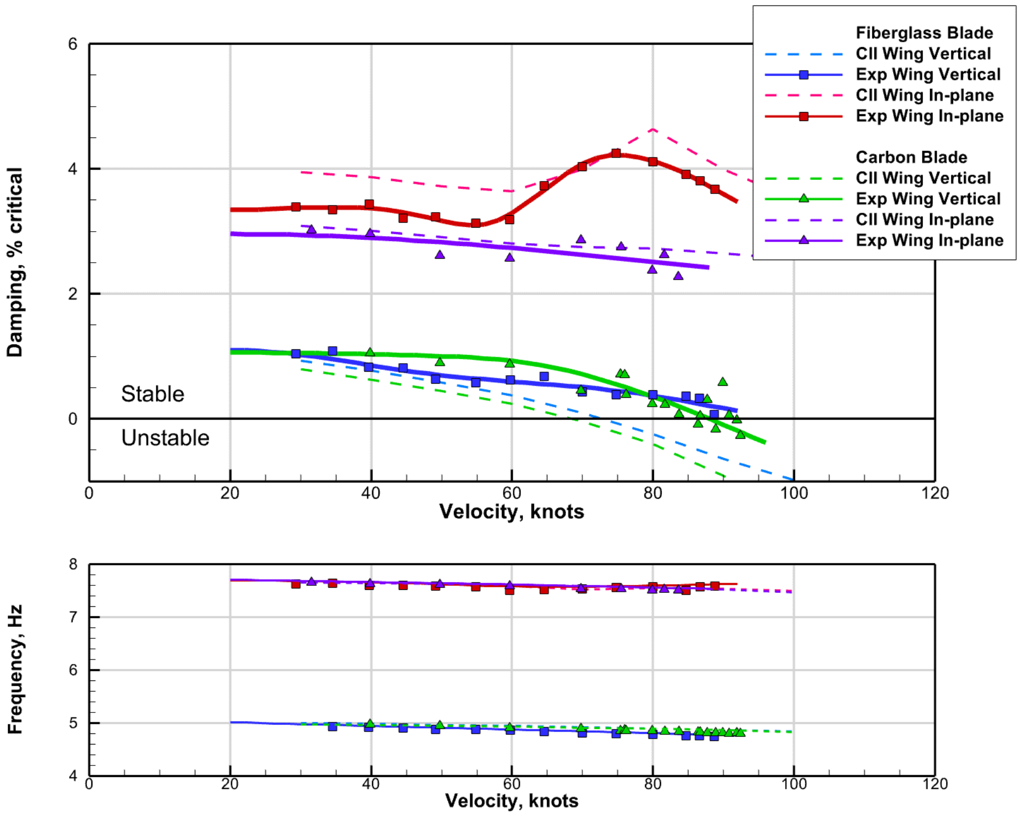

Figure 7. Comparison between the fiberglass and carbon-fiber rotors at 909 RPM with pitch-flap coupling (δ_3) of -30°.

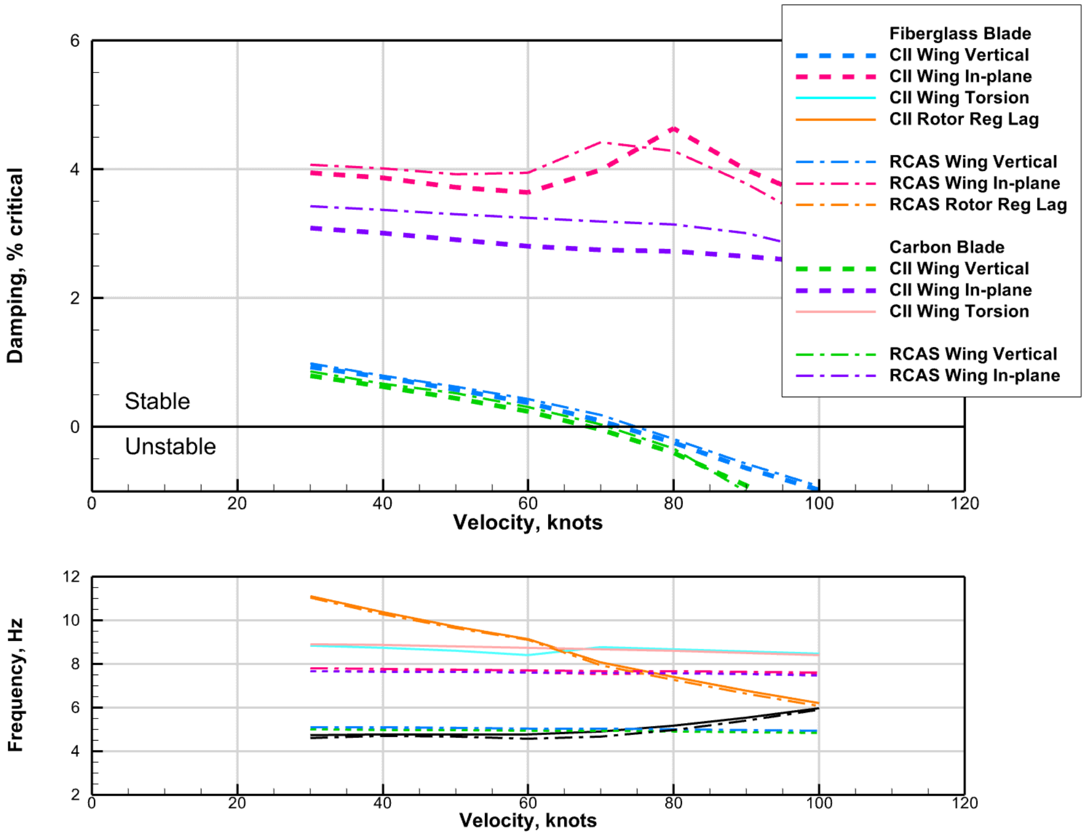

Figure 8. Analytical results for the fiberglass and carbon-fiber rotors at 909 RPM with pitch-flap coupling (δ_3) of -30°.

radial stations, unsteady thin airfoil theory, and lack of wing aerodynamics. More sophisticated approaches to all of these could improve correlations.

Figure 7 presents the frequency and damping for both the fiberglass and carbon-fiber rotor. The test data and analysis show that they have nearly identical stability boundaries. This is because the rotors are nearly the same except for flexibility of the rotor blades. The response of these two rotors involves the damping of the wing vertical mode monotonically decreases with increasing tunnel speed until it becomes unstable. This is an example of the Tiltrotor Whirl Flutter that was discussed above, where there are no blade modes to interact with the wing.

However, the reader will notice that although the in-plane mode damping is quite large there i s a significant difference in how the damping changes with airspeed. To highlight this, Figure 8 presents the analytical results for the same configurations, but with more rotor modes shown. The damping of all of these additional rotor modes is very high (>10%), but the frequencies start to intersect and interact as velocity increases. What can clearly be seen is that when the gimbal mode (black) intersects the wing vertical mode the wing vertical mode goes unstable. Since both blade sets have nearly identical wing-vertical and gimbal frequencies, this results in very similar instability boundaries. However, the regressive lag modes are very different between the two blade sets, with the frequency for the carbon-fiber rotor being off the scale (high) of Figure 8. For the fiberglass rotor, the regressive lag mode (orange) crosses the wing in-plane mode around 80 knots, causing the damping to increase. This is the second type of tiltrotor phenomenon, Proprotor Whirl Flutter.

Figure 9 presents the frequency and damping for both the fiberglass and carbon-fiber rotor for a pitch-flap coupling of -30° at a rotor speed of 727 RPM. A comparison between the two blade sets show they have nearly identical stability boundaries for the wing vertical mode for both the test data and analysis. The test data for the fiberglass rotor does show a dip in the damping around 85 knots, which is around the speed the rotor regressive lag starts to interact with the wing in-plane mode. However, this is not picked up by analysis. The carbon-fiber rotor demonstrated a higher damping than the fiberglass blade between 60 and 90 knots, though both are neutrally stable at around 107 knots.

Figure 10 illustrates the frequency and damping behavior of the carbon-fiber rotor for the pitch-flap coupling (δ_3) of -15° at a rotor speed of 909RPM. This configuration is similar to the pitch-flap coupling on the V-22 and XV-15. In this setup the measured stability speed increases by approximately 15 knots from the -30° δ_3 case. Similarly, analysis predicts a 20-knot increase. This increase results from a greater separation between the gimbal mode and the wing vertical bending mode for the -15° δ_3 case. The difference in the regressive lag frequency for the two pitch-flap couplings is presented in Figure 11. The results presented are the analytically predicted modes for the two cases. Experimentally the gimbal mode is very hard to determine since it is heavily damped. As can be seen from Figure 11 it is not necessarily a requirement for the gimbal mode to intersect the vertical bending mode to go unstable.

The pitch-flap coupling of (δ_3) of -15° demonstrate the largest disparity in stability boundaries when comparing the two blade sets. This results from the difference between Tiltrotor Whirl Flutter that occurs with the carbon-fiber rotor and the Proprotor Whirl Flutter that occurs with the fiberglass rotor. Figure 12 and Figure 13 illustrate these differences between the carbon-fiber and the fiberglass rotor for a rotor speed of 909 RPM and 727 RPM respectively with the pitch-flap coupling (δ_3) of -15°. This comparison highlights the largest difference between the two different types of stability. The response of the carbon-fiber rotor is akin to the Tiltrotor Whirl Flutter behavior, with no increase in damping due to the rotor flexibility. The response of the fiberglass rotor is clearly Proprotor Whirl Flutter with a large increase in damping as the regressive lag mode first intersects the wing in-plane mode around 70 to 80 knots. The frequency of the fiberglass rotor regressive lag mode continues to decrease until it intersects the wing vertical mode causing an increase in the damping above 100 knots. The analytical cases exhibit a significant underprediction, but the trend is similar where the fiberglass rotor flexibility causes an increase or bump in damping which extends the flutter boundary.

4. CONCLUSIONS

This paper discussed a subset of the second of wind tunnel test conducted on the Tiltrotor Aeroelastic Stability Testbed (TRAST) and provided critical insights into the dynamics of tiltrotor whirl flutter. This paper ultimately relates back to Reed's "Review of Propeller-Rotor Whirl-Flutter," Reference 5, with experimental testing showing the difference between a flexible blade and rigid blades with hinges. The TRAST testbed demonstrated that a stiff rotor is not ideal at high-speeds as the rotor flexibility increases the damping extending the stable region for the pitch-flap coupling of -15°. The pitch-flap coupling with -30° has such a low stability boundary it did not matter that the blades were very stiff.

This paper attempted to define the two types of tiltrotor whirl flutter phenomena:

Tiltrotor Whirl Flutter (Flapping Rotor & Airframe Pitch)

This type of instability involves only the gimbal and the airframe flexibility and can ignore the rotor flexibility. This type of instability is seen with the carbon-fiber rotor across all configurations.

Proprotor Whirl Flutter (Flapping/Blade/Airframe Pitch)

This type of instability involves the gimbal and the airframe flexibility but **cannot** ignore the rotor flexibility. This type of instability is seen with the fiberglass rotor at high tunnel speeds, specifically in this paper the pitch-flap coupling of -15°.

5. ACKNOWLEDGMENTS

The authors would like to acknowledge NASA's Revolutionary Vertical Lift Technology program, Aeroelasticity Branch and the Transonic Dynamics Tunnel for their contributions, effort, and support in acquiring the test data.

6. REFERENCES

1. Abbot, F.T., Kelly H, N., Hampton, K.D., "Investigation of Propeller-Power-Plant Autoprecession Boundaries for a Dynamic-Aeroelastic Model of a Four-Engine Turboprop Transport Airplane," NASA TN D-1806, Hampton, VA, Aug. 1963.
2. Kvaternik, R., "An Experimental and Analytical Investigation of Proprotor Whirl-Flutter," NASA Technical Paper 1047, December 1977.
3. Schroers, L. G., "Dynamic Structural Aeroelastic Stability Testing of the XV-15 Tilt Rotor Research Aircraft," NASA TM-84293 Moffett Field, CA. December 1982.
4. Popelka, D., Sheffler, M., Bilger J., "Correlation of Stability Test Results and Analysis for the 1/5 Scale V-22 Aeroelastic model" American Helicopter Society 41st Annual Forum, Fort Worth, TX, May 15-17, 1985.
5. Reed, W. H. III, "Review of Propeller-Rotor Whirl Flutter," NASA TR R-264, July 1967.
6. Akinwale, A., Datta, A., "High Speed Whirl Flutter Tests of the Maryland Tiltrotor Rig," Proceedings of the VFS 79th Annual Forum, West Palm Beach, FL, May 16-18, 2023.
7. O'Brien, N., Datta, A., "Aeroelastic Stability of a Hingeless Hub Tiltrotor at High Speeds," Proceedings of the VFS 80th Annual Forum, Montreal, Quebec, Canada, May 7-9, 2024.
8. Hoff, S., Fonte, F., Soal, K., Schneider, O., Kapteijn, K., "Whirl Flutter Testing of ATTILA Tiltrotor Testbed – Initial Results," Proceedings of the VFS 80th Annual Forum, Montreal, Quebec, Canada, May 7-9, 2024.

9. Kreshock, A.; Thornburgh, R.; Wilbur, M.; "Overview of the TiltRotor Aeroelastic Stability Testbed," Proceedings of the AIAA Science and Technology Forum and Exposition (AIAA SciTech 2022), San Diego, CA, January 3-7, 2022
10. Kreshock, A.; Thornburgh, R.; Wilbur, M.; Kang, H.; Piatak, D.; Sekula, M. "Initial Whirl-Flutter Characterization of the TiltRotor Aeroelastic Stability Testbed," Proceedings of the VFS 79th Annual Forum, West Palm Beach, FL, May 16-18, 2023
11. Thornburgh, R.; Kreshock, A., "Structural Modeling and Validation of the TiltRotor Aeroelastic Stability Testbed," Proceedings of the AIAA Science and Technology Forum and Exposition (AIAA SciTech 2024), Orlando, FL, January 8-12, 2024
12. Kang, H.; Kreshock, A.; Thornburgh, R.; Yeo, H.; Shen, J.; "Correlation of Tiltrotor Aeroelastic Stability Wind Tunnel Test," Proceedings of the VFS 79th Annual Forum, West Palm Beach, FL, May 16-18, 2023
13. Yeo, H., and Kreshock, A., "Whirl Flutter Investigation of Hingeless Proprotors," Journal of Aircraft, Vol. 57, No. 4, July 2020.

7. CLASSIFICATION & COPYRIGHT

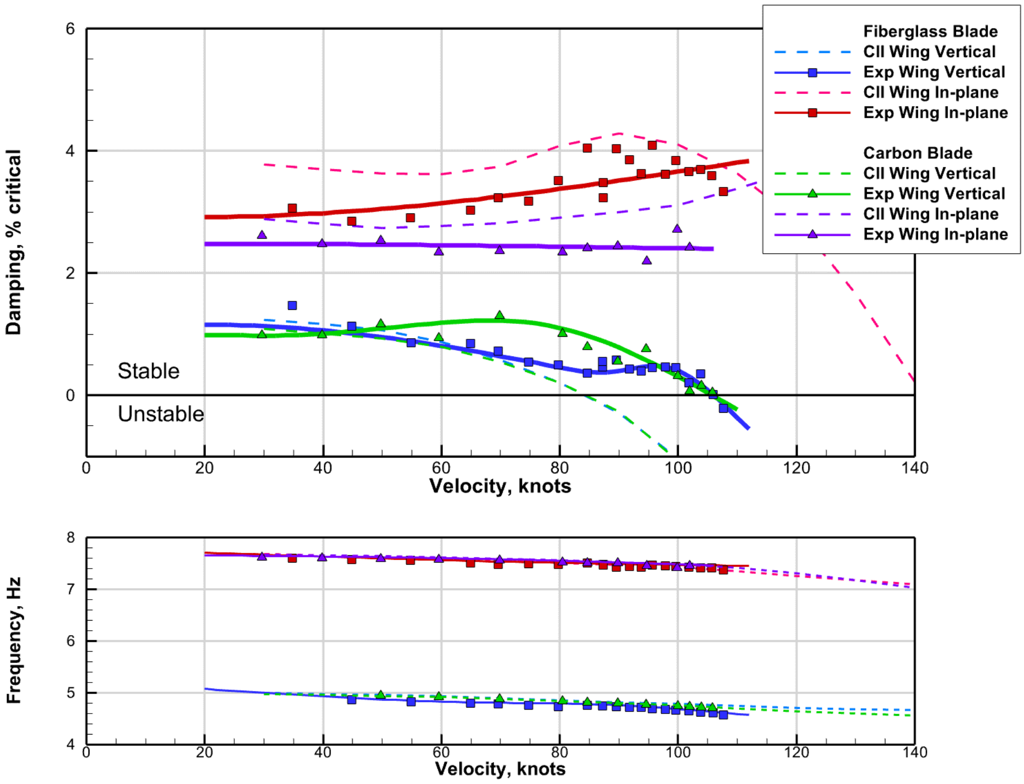

Figure 9. Comparison between the fiberglass and carbon-fiber rotors at 727 RPM with pitch-flap coupling (δ_3) of -30°.

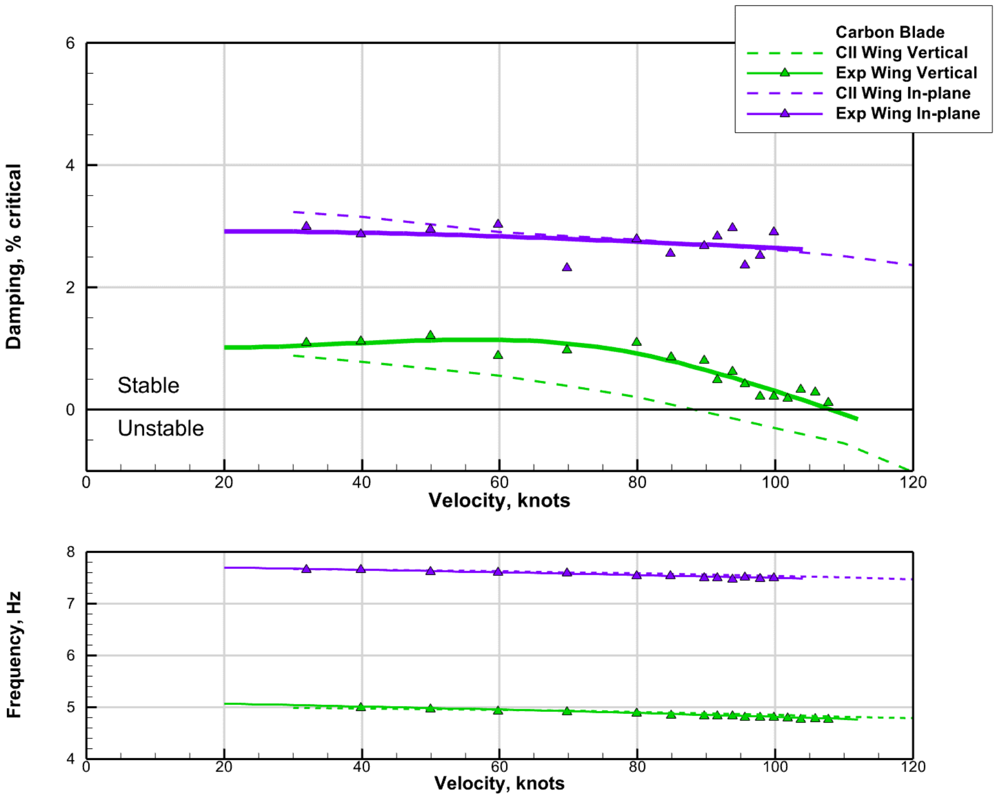

Figure 10. Frequency and damping test data and analytical results for a pitch-flap coupling (δ_3) of -15° and carbon-fiber rotor at 909 RPM.

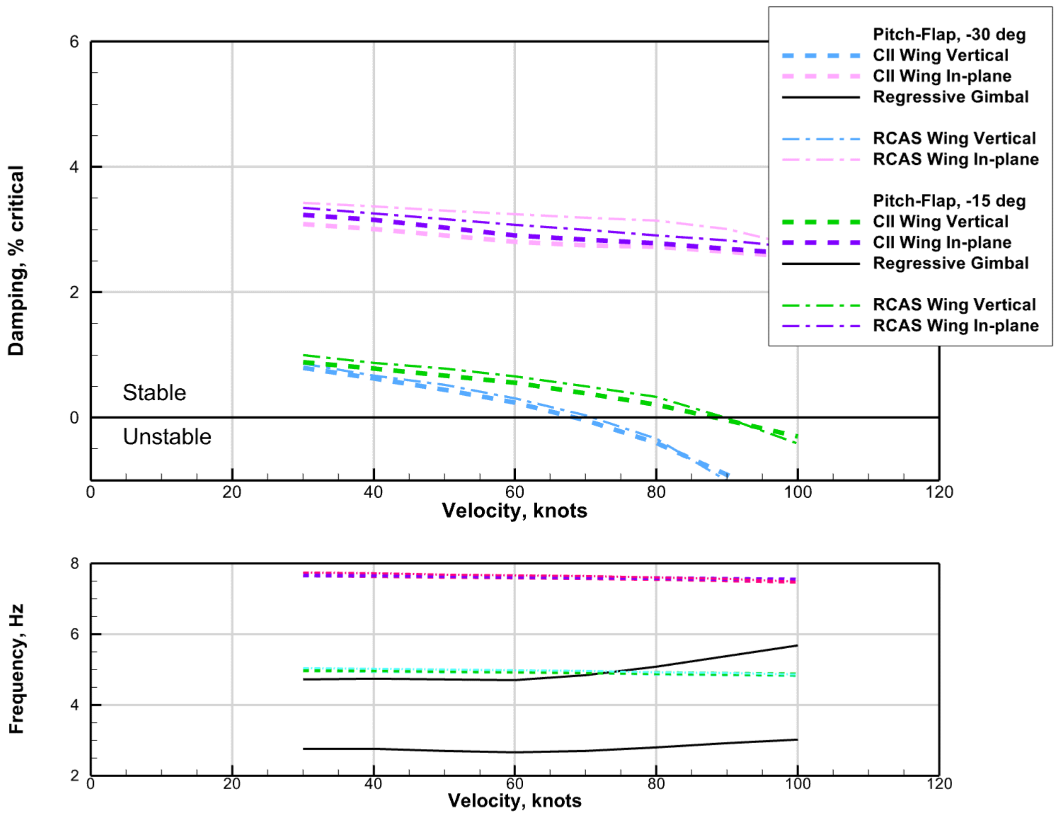

Figure 11. Frequency and damping from analysis for the carbon-fiber rotor at 909 RPM, a comparison of pitch-flap coupling.

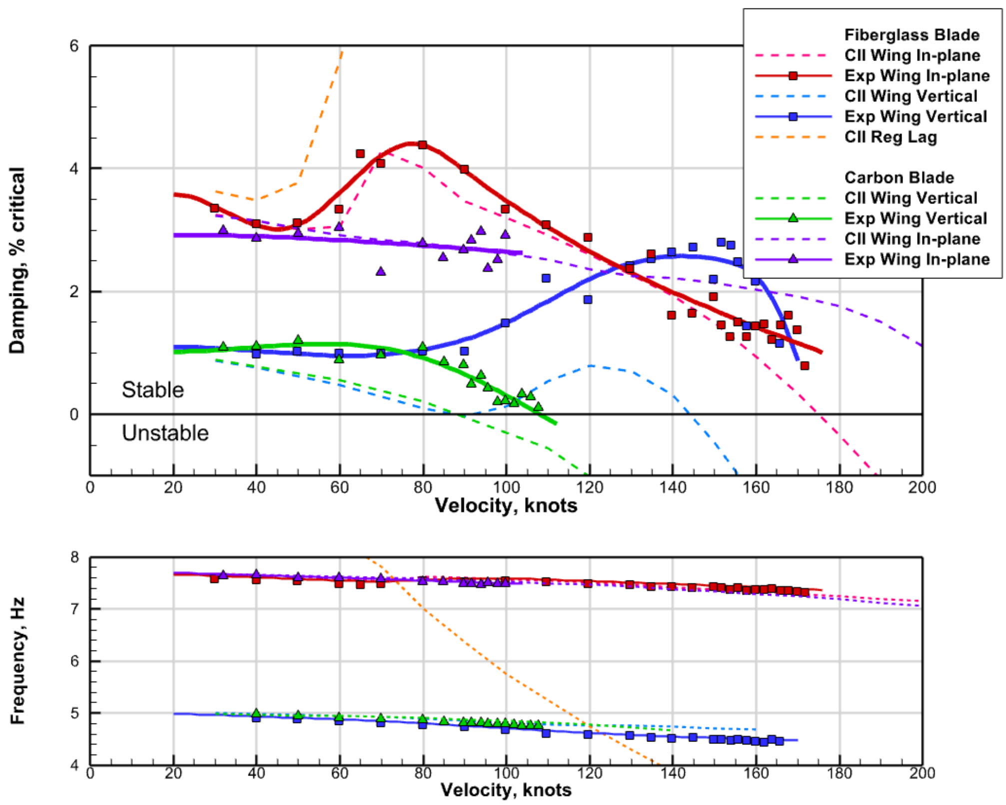

Figure 12. Frequency and damping test data and analytical results for a pitch-flap coupling (δ_3) of -15° with fiberglass and carbon-fiber rotors at 909 RPM.

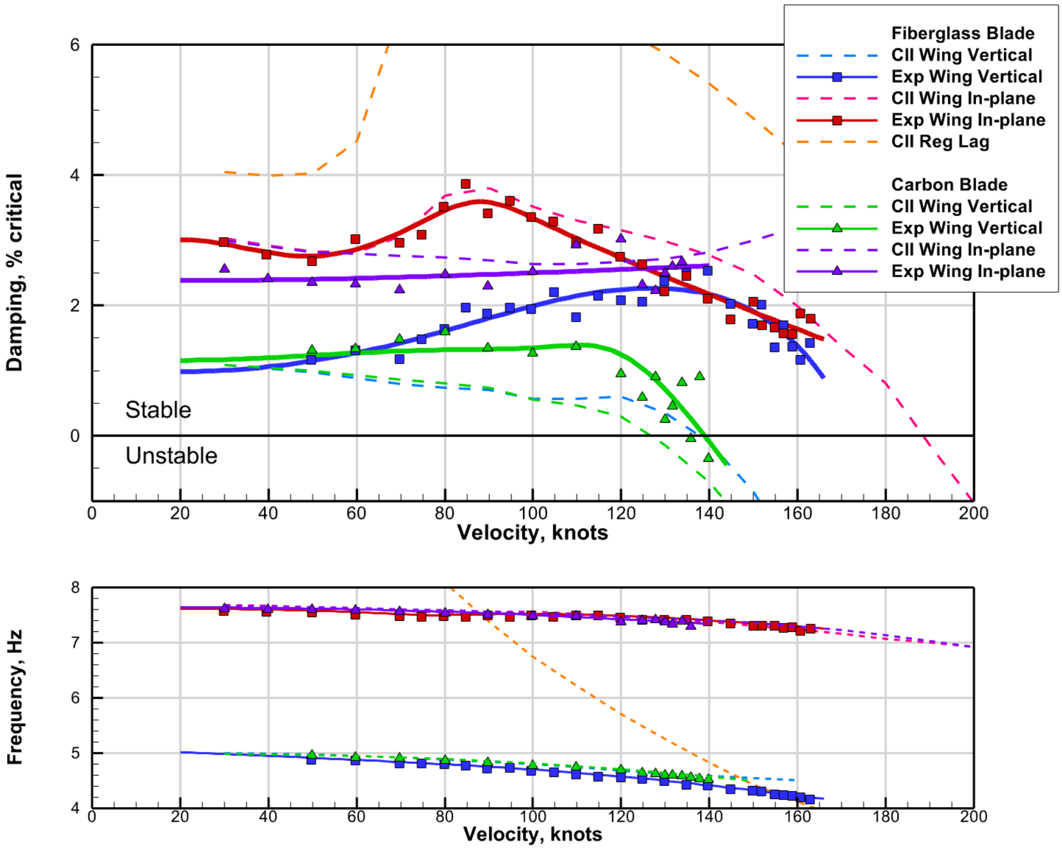

Figure 13. Frequency and damping test data and analytical results for a pitch-flap coupling (δ_3) of -15° with fiberglass and carbon-fiber rotors at 727 RPM.